PERGAMON

Journal of Atmospheric and Solar-Terrestrial Physics 65 (2003) 379–390

Journal of ATMOSPHERIC AND SOLAR-TERRESTRIAL PHYSICS

www.elsevier.com/locate/jastp

Studies of equatorial F-region depletions and dynamics using multiple wavelength nightglow imaging

G.K. Mukherjee*

Indian Institute of Geomagnetism, Colaba, Mumbai 400 005, India

Abstract

A charge coupled device based all-sky imaging system with 180° field of view has been operating at Kolhapur (16.8°N, 74.2°E, dip lat. 10.6°N) in India on clear moonless nights to study the dynamics of equatorial ionospheric irregularities by examining the images of three oxygen lines at OI 630, 557.7 and 777.4 nm. The all-sky camera offers broad and instantaneous coverage of the movement of large-scale size ionospheric irregularities (depletions or bubbles) over a region of 1800 km at about 300 km altitude. The location of the station is important as the single image at a given instant maps the irregularities over a large area extending from the geomagnetic equator to the equatorial ionization anomaly region. Several characteristics of irregularities discussed in this report were observed during ISTEP campaign periods conducted in March–April of 1998 and 1999. One example of the signature of simultaneous depletions observed in OI 630, 557.7 and 777.4 nm images is reported. Also, the signature of midnight temperature maximum (MTM) in OI 630 nm airglow has been presented. The tilt of the MTM structure with magnetic meridian was found to change during the course of its movement towards north. The eastward plasma drift speeds ranging from 0 to 289 m/s computed from bubble movement matches well with the drift speeds computed from VHF scintillation experiments and Jicamarca radar observations.

Keywords: Equatorial spread-F; Depletion; MTM; Apex altitude; Equatorial ionization anomaly

1. Introduction

The observations of Ionospheric plasma irregularities associated with nighttime equatorial spread-F phenomena have been extensively carried out at different longitudes in a wide range of altitude, starting from the base of the F-region to region beyond 1000 km in the last three decades by using both radio techniques (incoherent back-scatter radar, rockets, satellites and UHF/VHF scintillation, ionosondes, topside sounder) and optical techniques (conventional tilting and scanning photometers and wide-angle imaging system) (Weber et al., 1978; Fagundes et al.,1999; Kil and Heelis, 1998; Mendillo et al., 1997; Singh et al., 1997; Tsunoda, 1985; Sahai et al., 1996; Malcolm et al., 1984; Taylor et al., 1997; Mukherjee et al.,1998; Mukherjee, 2002; Sinha et al., 2001; Tinsley et al., 1997).

* Corresponding author.
E-mail address: gkm@iig.iigm.res.in (G.K. Mukherjee).

The tropical atomic oxygen nightglow arising from recombination of plasma in the F-layer has been used to map the large-scale F-region plasma irregularities or depletions (transequatorial bubbles or plumes). The scale size of the structures varies between 10s of centimeters to 100s of kilometers, which are very sensitive to a wide range of diagnostic techniques (Abdu, 1993). The wide-angle optical imaging technique of F-region nightglow emissions has been used by several research workers to study the large-scale equatorial plasma irregularities (Weber et al., 1978, 1980, 1982, 1983; Sinha and Raizada, 2000; Mendillo and Baumgardner, 1982; Mendillo and Tyler, 1983; Rohrbaugh et al., 1989; Sahai et al., 1994; Mukherjee, 2002). These are the regions where the plasma densities decrease abruptly by several orders of magnitude compared to the ambient plasma densities. The HF communications and satellite to ground communication, navigation systems based on GPS satellites get affected by these plasma irregularities. Weber et al. (1978) observed the first images of magnetically N–S aligned

1364-6826/03/$ - see front matter
PII: S1364-6826(02)00214-6

structures of low-intensity (depletions) OI 630 nm airglow during the period of spread-F observations. These low-intensity regions are the optical signatures of depletions, which have been, mapped in the all-sky images of OI 630.0, 557.7 and 777.4 nm emissions. It is generally initiated by plasma instability processes operated at the bottom side of the F-region after sunset under certain conditions when the bottomside of the F-layer becomes unstable for the growth of a fluid type gradient instability mechanism such as gravitational Raleigh–Taylor instability (Dungey, 1956) in conjunction with $E \times B$ instability (Martyn, 1959) with seeding provided by gravity waves, vertical winds, electric fields, etc. (Singh et al., 1997).

Owing to much greater conductivity parallel to the magnetic field lines than perpendicular to them, plasma in the magnetic field tubes tend to convect along F-region magnetic field lines while growing upwards and hence the depleted plasma regions tend to be field aligned. They often get tilted in westward direction while moving towards the east. At the boundaries and within the depletions, small-scale size irregularities (∼meter to kilometer size) are generally produced which give rise to strong VHF nighttime scintillations in satellite beacon signals. As these bubbles move buoyantly upward with respect to the ambient plasma in the equatorial region, their bottom-side feet migrate poleward, reaching dip latitudes of over ±15°. During this period, the vertical motion is driven by the gravitational Rayleigh–Taylor mechanism and in the process the depleted flux tubes can reach altitude well over 1500 km at the magnetic equator which is known as the apex height of the bubbles. They generally break up into smaller-scale size electron density irregularities, which are associated with spread-F, backscatter and UHF/VHF scintillation. The use of all-sky optical imaging systems has been especially important in studying the spatial extent of the bubbles and their motion relative to both the ground and to the surrounding ambient ionosphere (Mendillo et al., 1997). A charge coupled device (CCD) based all-sky imaging system (180° of view) developed in collaboration with Boston University, US, was operated from Kolhapur (16.8°N, 74.2°E, dip lat. 10.6°N) on clear moonless nights to obtain the signature and dynamics of plasma bubbles by studying the images at OI 557.7, OI 630.0 and OI 777.4 nm. The data for the generation and evolution of these large-scale irregularities are limited at the Indian longitude sector (Mukherjee et al., 1998). The location of the observing station is important as a single image frame at a given instant provides information regarding the dynamics of these irregularities over a large low-latitude region starting from geomagnetic equator to the equatorial inonization anomaly (EIA) region. As discussed by Mendillo et al. (1997), the imaging studies provide a wealth of information, which are not provided easily by other ionospheric diagnostic experiments.

We present and discuss in this report several characteristic features of simultaneous ground-based optical and radio diagnostics of large-scale equatorial F-region plasma irregularities carried out from a low-latitude station, Kolhapur, in India situated close to equatorial ionization anomaly region during the period of moderate solar and geomagnetic activity.

2. Tropical nightglow emission

The spectral line at OI 630 nm is indicative of dissociative recombination involving O_2 molecules and electrons near 300 km altitude (Mukherjee and Dyson, 1992) in the F-region and is metastable $O(^1D)$ state which is formed in the dissociative recombination of O_2^+ and electrons ($O_2^+ + e \to O + O^*$) in the F-region (Peterson and Van Zandt, 1969). The O_2^+ is produced from charge transfer of O^+ with O_2 and observed OI 630 nm emission is the column integral ($\int n(O^+)n(O_2)\,ds$) of the product of O^+ and O_2 concentration. The major portion of OI 557.7 nm emission comes from the recombination of oxygen atoms in the mesopause region (80–100 km). There is a general agreement that the OI 557.7 nm emission is excited by the so-called two-step energy transfer process $O + O + M \to O_2^* + M$, $O_2^* + O \to O_2 + O(^1S)$ (Bates, 1981). A fraction of these emissions also originates from the dissociative recombination process in the F-region. It is estimated to be about 20% of the F-region 630 nm contribution (Sobral et al., 1992). Only difference is that lifetime of $O(^1D)$ state is 178 s against $O(^1S)$, which is almost 0.9 s.

The OI 777.4 nm emission is a prompt emission (Tinsley and Bittencourt, 1975) from $O(^5P)$ state which is formed due to radiation recombination of O^+ with electrons process ($O^+ + e \to O^* + h\nu$ (777.4 nm)) and since at F-region heights, the O^+ concentration is essentially equal to the electron concentration, the observed OI 777 nm emission rate is proportional to $\int n(O^+)^2\,ds$. Thus, the OI 777 nm emission is independent of the layer height but depends on the square of concentration near the peak of F-layer and there by providing an indirect measurement of F-region peak electron densities, n_m (e).

Generally, OI 777 nm emission is weaker than OI 630 nm emission at low-latitude region. The ratio of $(I_{777})^{1/2}/I_{630}$ is a measure of the height of the F-layer. The use of these oxygen emission lines in studying the F-layer properties has been discussed by Tinsley and Bittencourt (1975) and Bittencourt et al. (1983).

3. Instrumentation

3.1. All-sky camera

The design features of a CCD-based imaging system have been explained by a number of research workers (Baumgardner and Karandanis, 1984; Mendillo et al., 1989) and more recently by Mendillo et al. (1997), Mukherjee et al. (1998) and Nakamura et al. (1999).

Table 1
Filter details and exposure times

Wavelength (nm)	Diameter of the filters (in)	Bandwidth (nm)	Transmission (%)	Integration time (s)
OI 630	4	1.0	65	60
OI 557.7	4	1.0	65	60
OI 777.46	4	1.0	65	60

There are six filter positions, which can be used to study various emission lines originating at different ionospheric–thermospheric heights. At present, we are using three oxygen line filters: 630.0, 557.7 and 777.4 nm along with a background filter. The details about the filters and the exposure time used are given in Table 1. Since our main concern is to study F-region dynamics at night, we concentrate mainly on spatial and temporal characteristics of OI 630 nm emission. The superiority of CCD over almost all other image forming devices has been well established in the last two decades due to its high resolution, high quantum efficiency, broad spectral response, low noise and large dynamic range (Abreu and Skinner, 1989; Janesick and Blouke, 1987).

4. Geometry of observations

Fig. 1 shows the location of the observing station Kolhapur with respect to geographic coordinates. The two circles indicate the coverage of the camera system for zenith distances 75° and 90° for an emission height of 300 km. Fig. 2 shows the 75° zenith angle distance of 300 km height which encompasses approximately 8° of latitude longitude from the zenith which is equivalent to a horizontal diameter of ~1800 km through the zenith at 300 km. Between zenith angles 75–90°, an additional 8° latitude/longitude are encompassed. Due to compression effects these regions are not very accurate for image analysis. It is important to note, however, that the geomagnetic equator falls within 75–90° zenith angles and appears near the southern edge of the field of view. Fig. 3 shows the image overlay pattern as seen from Kolhapur. The north–south aligned motions of the bubbles can be used to find the bubble altitude above the magnetic equator considering that the layer is situated at 300 km. A depleted region reaching the extreme northern edge of the image will correspond to an altitude greater than 1500 km above the equator. To illustrate the typical nightglow images (630.0 nm) and explain F-region dynamics involving small- and large-scale irregularities we also use measurements from ionosondes, VHF scintillation and photometric experiments.

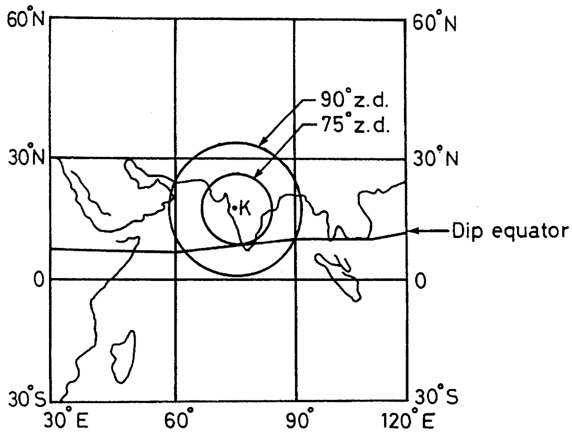

Fig. 1. Field of view at 75° and 90° zenith angles at 300 km for the all-sky camera at Kolhapur.

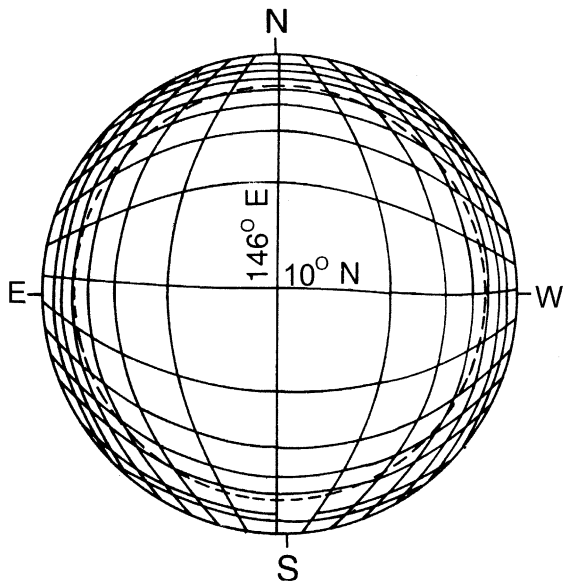

Fig. 2. Dip latitudes and magnetic longitudes of geomagnetic field lines at 2° interval observed at 300 km altitude at Kolhapur.

5. Results and discussion

5.1. Observation on March 25–26, 1998

The solar flux (F10.7 cm) for the day was 114 units and the average Kp was 3.35. This was a night of moderately

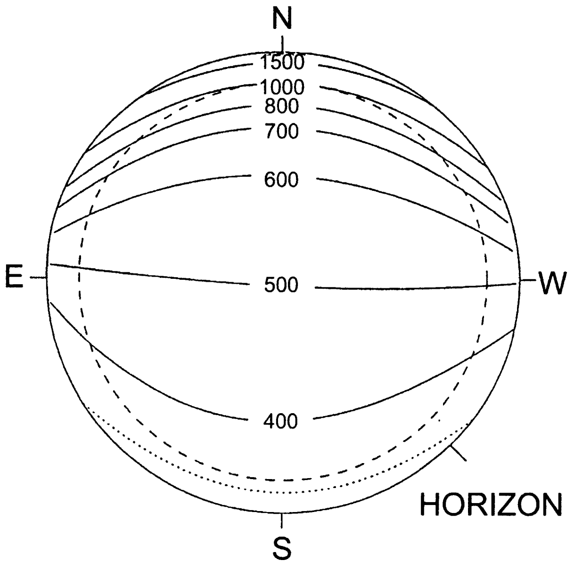

Fig. 3. Projected altitude over the equator for OI 630.0 nm emission at 300 km for Kolhapur situated at the center. Dotted line represents the magnetic equator; dashed line represents a 75° zenith distance.

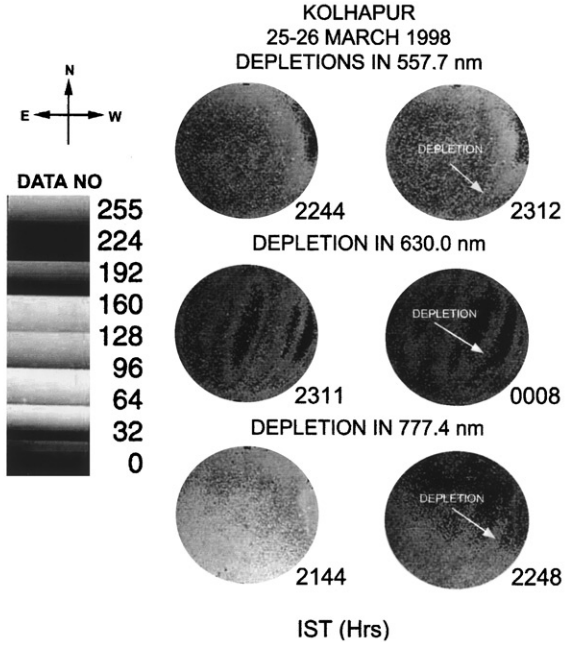

Fig. 4. Simultaneous depletions observed in OI 557.7, OI 630 and OI 777.4 nm on the night of March 25–26, 1998.

disturbed condition with a moderate solar activity. All-sky images were taken with 630.0, 557.7 and 777.4 nm filters at every 1-min interval. On the night of March 25, 1998, a series of north–south aligned depletions were seen. Also, simultaneous depletions were seen in all three-emission lines (OI 630.0, 557.7 and 777.4 nm) (Fig. 4). It was a typical spread-F night. The depletions were very prominent in OI 630 nm emission line compared to other two oxygen lines. The north–south aligned plasma depletions were observed from 21:30 to 01:00 h during the night.

In order to find the depth and width of depletions, we scan several images from east to west (through zenith) direction after flat fielding them and calculate OI 630 nm intensity at each pixel. In Fig. 5 we depict the OI 630 nm intensity profile from 2308 to 2341 IST h (IST=UT+5.5 h) when depletions observed were strong and showed variabilities in shapes and sizes. The depth of bubbles (depletions) was estimated to be varying between 30% and 50% and the width of the bubbles was ranging between 50 and 350 km. At 2334 h the western wall of the depletion region showed ripples with wavelength of about 38 km, which could be due to propagation of standing waves between the center of the depleted region and the western wall reaching the background high-intensity region. Based on the airglow and Ionosonde measurements, Weber et al. (1982) showed such a representative structure in the plasma depletion region on the western wall of a crest or elevation in the bottom side of the F-layer. The apex altitude of the bubbles at the equator reached a height more than 1500 km while moving from west to east. The depth of depletions was stronger in OI 630.0 and OI 557.7 nm than in OI 777.4 nm emission (not shown in the diagram). There is a time lag between depletion observed in OI 630.0 nm and other two lines. This could be due to resolving power of the imaging system, the relative intensity and the lifetime of the emission lines studied. The continuous sequence of images helps to identify the eastern and western edges of the depletions as they drift eastwards. Using the latitude and longitude grids of the geomagnetic field lines for an assumed emission height of 300 km, eastern and western edges of the depletions were determined from successive images during the night as the sequence of images provides a continuity of identification of bubble characteristics. By comparing successive images, the speed and direction of the airglow features (bubbles) were measured as a function of local time. Fig. 6 shows the typical drift profile during nighttime between 2130 and 01:00 IST. The speeds were derived from the depletion region marked by an arrow in the diagram and it was found that the drift speeds decrease steadily during the pre-midnight hours reaching minimum values around midnight and subsequently accelerated up to 50 m/s. The drift speeds compare well with the earlier imaging observations of drift motions of F-region depletions above the magnetic dip equator at Alcantara (2.3°S, 44.5°W) in Brazil (Taylor et al., 1997) and also from the Jicamarca incoherent scatter radar data base for solar 10.7 cm flux index < 100 (Fejer et al., 1991). Taylor et al. (1997) also provided examples of the reversal of the bubble drift motion from east

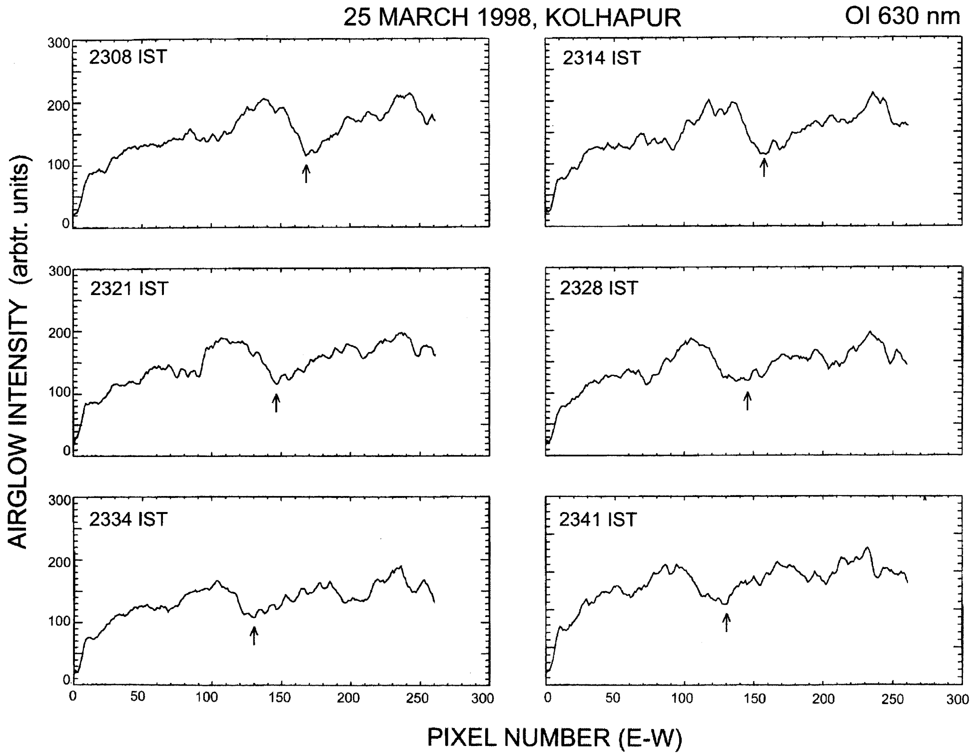

Fig. 5. East–west scans of OI 630 nm intensity at the equatorial plane of the successive images observed at 2308, 2314, 2321, 2328, 2334 and 2341 h on the night of March 25, 1998 showing the changes in the width and depth of depletion (structure is marked by an arrow).

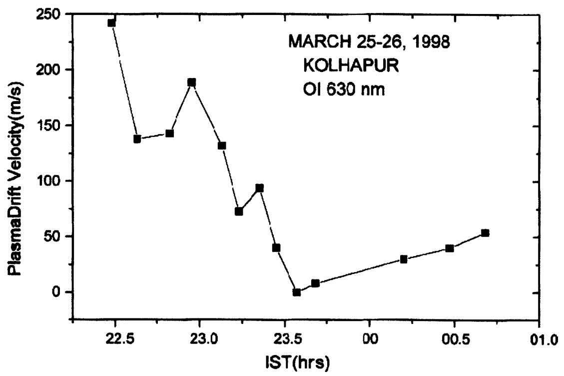

Fig. 6. Variation of zonal plasma drift velocity (m/s) as a function of local time during the night of March 25–26, 1998.

to westward direction and explained the phenomena as due to reversal of normal F-layer dynamo electric field at night. Though our measurements of zonal plasma drifts show the similar trend at night, the drift speed never became negative after reaching the minimum value. The sluggish nature of drift speeds at the middle of the night could be due to modification of F-region dynamo electric field due to magnetic disturbance.

5.1.1. Comparison of optical data with magnetic record

The geomagnetic field (H, Z, and D) data discussed in this report were obtained from a nearby station, Alibag (18.63°N, 72.87°E). Fig. 7 shows the variation of geomagnetic field components (H, Z, and D) as a function of local time (IST). It is noticed that a geomagnetic storm (gradual commencement (GC) type) was in progress commencing at 15:30 h (IST). The maximum value of the Dst excursion took place around 21:30 h, thereafter the activity started diminishing up to 1 O'clock at night. It is interesting to observe when $\mathrm{d}H/\mathrm{d}t$ was positive during the period 21:30–00:30 h at night, at the same time interval depletions in OI 630 nm images were observed at the station. A reversal of normal nighttime downward drift of the F-layer to the upward direction is required to generate these irregularities (Aarons, 1991). At night, zonal westward electric fields produce a downward vertical drift. The effect, however, of the ring current in the midnight and post-midnight period when the layer height is normally decreasing and the electric field is westward, is to create for a short time an eastward electric field which raises the height of the layer for shorter period of time, the layer height then falls after creating the irregularities. For the growth of irregularities under magnetically disturbed conditions a reversal of the normal nighttime downward drift of the F-layer to upward direction is required.

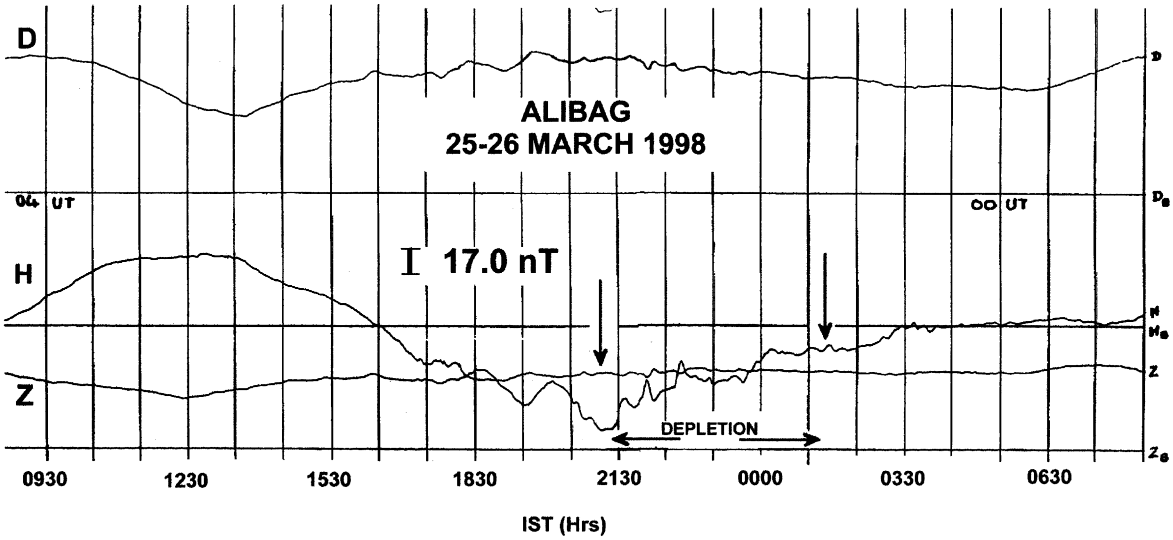

Fig. 7. Magnetogram of Alibag (18.63°N, 72.87°E) shows H, D and Z variations for the night of March 25–26, 1998.

5.1.2. Investigations of OI 557.7 *and OI* 630 nm *nightglow intensity ratios during the occurrence of equatorial F-region plasma bubbles*

It is well known that ground-based observations of OI 557.7 nm emission line receives two contributions to the integrated intensity emanating from two layers (from mesospheric E-region (90–100 km) and the thermospheric F-region heights (250–300 km)). Several investigators (Chiplunkar and Tillu, 1970; Rao and Kulkarni, 1974; Sobral et al., 1992) have investigated the F-region component of the OI 557.7 nm emission at low latitudes. For comparison of intensities of mesospheric OI 557.7 nm emissions in relation to other emissions such as OH and molecular oxygen bands, it is necessary to have an estimate of the F-region component. Using the photometric data of simultaneous depletions in OI 557.7 and OI 630.0 nm, the F-region contribution has been estimated to be 26% of that of the OI 630.0 nm intensity by Fagundes et al. (1995). We present here the estimate of the F-region component to OI 557.7 nm from the near simultaneous observations of the depletions in OI 557.7 and OI 630.0 nm through all-sky imaging, respectively. We use the method adopted by Fagundes et al. (1995). Following their approach, we define a ratio r between the difference of OI 630.0 and OI 557.7 nm intensities before and during the passage of plasma bubble as

$$r = (\Delta I_{557.7(\mathrm{E})} + \Delta I_{557.7(\mathrm{F})})/\Delta I_{630.0(\mathrm{F})} \approx \Delta I_{557.7(\mathrm{F})}/\Delta I_{630.0(\mathrm{F})}$$

assuming that contribution to $I_{557.7}$ from E-region remains the same before and during the passage of plasma bubble ($I^{\mathrm{B}}_{557.7(\mathrm{E})} \approx I^{\mathrm{F}}_{557.7(\mathrm{E})}$).

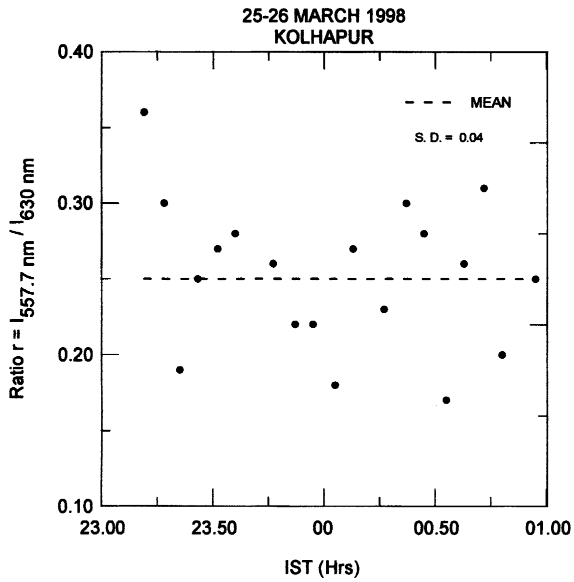

Fig. 8. Ratio r ($\Delta I_{557.7(\mathrm{F})}/\Delta I_{630(\mathrm{F})}$) as a function of local time on the night of March 25–26, 1998.

The local temporal variations of both OI 630.0 and 557.7 nm emissions show simultaneous and similar intensity depletions when a plasma bubble moves across the field of view of the all-sky camera. The passage of plasma bubble modifies the F-region contributions of the OI 557.7 and OI 630.0 nm intensities and this ratio is proportional to $I_{557.7(\mathrm{F})}/I_{630.0(\mathrm{F})}$. The computed ratio r is plotted in Fig. 8 as a function of local time. The mean F-region contribution turns out to be $25 \pm 4\%$ to OI 557.7 nm

5.2. Zonal plasma drift measurement

Using the latitude and longitude grid of the geomagnetic field lines at 2° interval for an assumed height of 300 km, the eastern and western edges of the depletion were determined from successive images. The spatial separation and their time delay were noted and thereby the eastward depletion drifts were estimated and they were plotted as a function of local time. Fig. 9 shows typical drift profiles for three nights in March 99 (upper panel) and April 99 (middle panel). Magnetic activity index Ap and solar F10.7 cm flux values were also depicted in the figure. The lower panel shows the observed average zonal behavior for March and April 1999 along with the mean eastward component wind velocity using HWM93 model (Hedin et al., 1996). On the basis of theoretical considerations, it is suggested that nighttime plasma drifts near the equator are approximately equal to F-region neutral winds (Rishbeth, 1971; Biondi et al., 1988). Therefore, with this consideration in mind, we intend to compare the mean observed zonal component of the bubble velocity with eastward component of F-region neutral wind. For numerical computation of wind velocity we use the Hedin's improved version (Hedin et al., 1996) of the model (Hedin et al., 1991) for March and April 15, 1999 at Kolhapur with appropriate parameters. The model

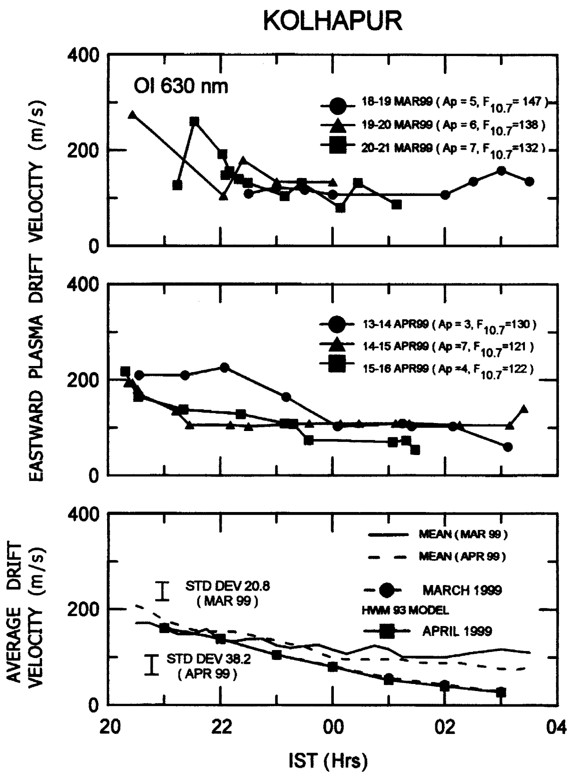

Fig. 9. Variation of nighttime F-region plasma drifts as a function of local time (IST) during March and April 1999.

predictions agree very well with the observations at night. It can be seen that on the average, the drift speeds decrease steadily reaching their minimum value during post-midnight hours. This also compares well with the equatorial zonal neutral wind flow measurements by WATS (wind and temperature spectrometer) aboard DE-2 satellite in 1981 as well as ground-based zonal ion drift measurement by the Jicamarca incoherent radar for the corresponding period (Fig. 12 in Herrero et al., 1993). This behavior matches well with OI 630 nm measurements of F-region plasma drifts as observed by Taylor et al. (1997) from an equatorial station Alcantara (2.3°S, 44.5°W) in Brazil.

Kumar et al. (1995) also estimated the zonal drifts of the ionospheric irregularities computed from the time delays in the onset of similar scintillation patches at a pair of stations, Ujjain and Bhopal, situated exactly at the same latitude in the Indian anomaly region. The calculated eastward velocities of the irregularities found by them varied between 180 and 55 m/s during the course of night. At the same longitude sector, Koparkar (1988) estimated east–west drift speeds to vary from about 170–60 m/s and Chandra et al. (1989) found 300–100 m/s during the course of night. Similar findings were also reported by Basu et al. (1991) by comparing irregularity drifts with neutral wind.

Anderson and Mendillo (1983) showed that in the absence of significant contribution from E-region horizontal current flows and tidally driven polarized electric fields, the equatorial zonal nighttime plasma drift is given by

$$V_{\mathrm{E}} = \int \sigma_{\mathrm{p}} UB \,\mathrm{d}s/B \int \sigma_{\mathrm{p}} \mathrm{d}s,$$

where σ_{p} is the Pederson conductivity, U is the zonal neutral wind velocity, B is the magnetic field intensity and the integration are performed from one end of the field line to the other. It is seen that the height profile of the flux tube integrated Pederson conductivity can significantly affect the amplitude and altitudinal variation of the zonal plasma drifts.

5.3. Signatures of midnight temperature maximum

There are cases when the measurements both by ground-based and satellite-borne instrumentation, revealed a pronounced increase in the neutral temperature around midnight over the equator, sometimes the value exceeds the afternoon maximum (Spencer et al., 1979). This feature is known as the midnight temperature maximum (MTM), a region of anomalous temperature and density that is generally considered to result from atmospheric tidal interactions. Winds generated due to pressure bulge phenomena propagate poleward (northward) and its vertical component moves the F-region plasma downward to region of enhanced loss and airglow production. This event is prominent at the stations during the months of March and April around local midnight. As pointed by Mendillo et al. (1997), an all-sky camera can be used to map the movement of the transient airglow structure (brightness wave (BW))

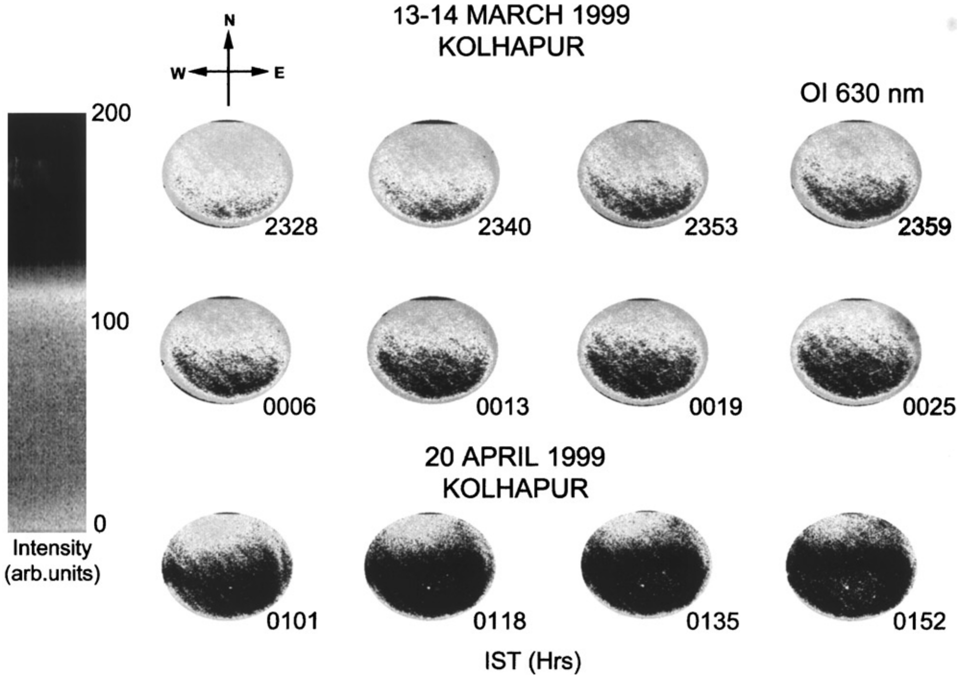

Fig. 10. Signature of MTM (brightness wave) as observed in OI 630-nm nightglow images on the night of March 13–14 and April 19–20, 1999.

caused due to MTM-induced winds propagating across the all-sky field of view from equator to poles. Fig. 10 shows two examples of the sudden enhancement in brightness that first appears at the magnetic equatorial region in east–west direction and moves towards the north with a phase velocity 248 and 150 m/s on March 13–14 and April 19, 1999. It was noticed that there was a tilt in the structure with the magnetic meridian and the structure changes as it moves towards north. The structures were prominent for about 2–3 h during post-midnight period. Fig. 11 shows the OI 630 nm images during the night of February 5, 2000 depicting strong enhancement similar to brightness wave moving from southwest to Northeast direction at 2302, 2310, 2317, 2324, 2332, 2339, 2346 and 2353 h IST. The brightness pattern in OI 630 nm continued for more than an hour and could be a signature of MTM moving towards northeast direction with a phase velocity of 190 m/s first registering their signature in the equatorial region. The enhancement and the brightness region are approximately tilted to the meridian by 45°. As described by Colerico et al. (1996), an MTM pattern fixed to local time at the observing site induces a meridional wave moving with a phase speed and

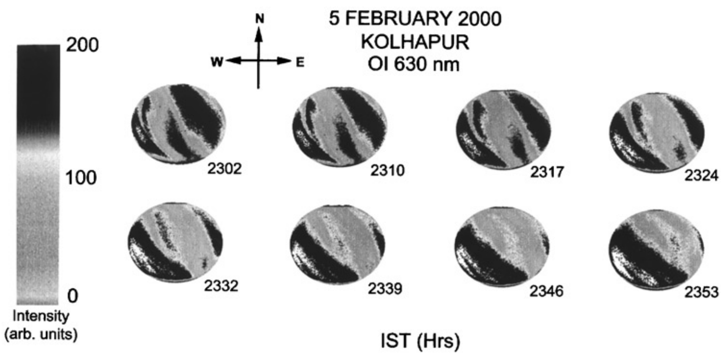

Fig. 11. Signature of MTM (brightness wave) as observed in OI 630-nm nightglow images on the night of February 5, 2000.

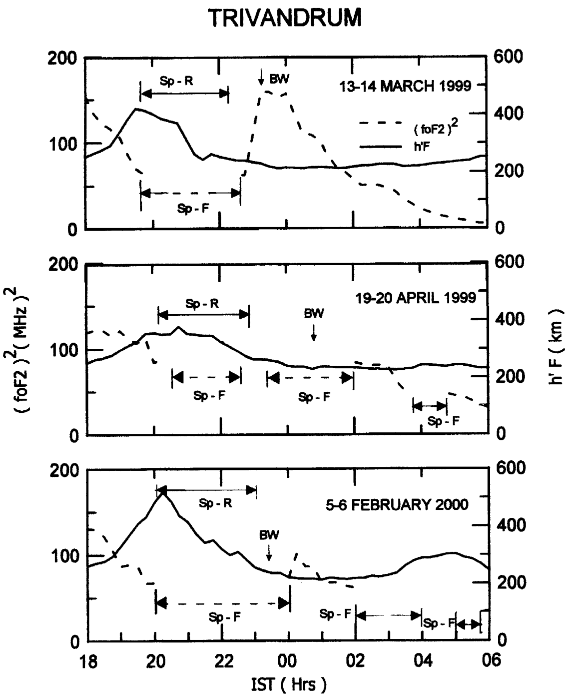

Fig. 12. Ionosonde h'F and f_0F_2 measurements taken at the Trivandrum station for March 13–14, April 19–20, 1999 and February 5–6, 2000 showing enhancement of electron density and small dip in the F-layer height, h'F during MTM events.

the imaging system corotates with corotational speed of the earth V_{co} being related to the tilt (θ) of the MTM structure with respect to the meridian.

$$\tan\theta = V_{co}/V_{sn},$$

where V_{sn} is the apparent meridional velocity by which the BW structure moves in the field of view.

Such tilt angles of MTM have been reported by (Herrero and Spencer, 1982, 1983) and Colerico et al. (1996). This feature is also dependent on solar activity. We found the tilt angle to be about 45° towards west for OI 630.0 nm. However, the signature was missing in images of OI 557.7 and 777.4 nm on these nights. This was the first observation of MTM from this part of the globe using an all-sky camera. The study would help us to examine further the latitudinal and longitudinal variation of day-to-day variability of MTM pressure bulge phenomena in Indian longitude sector, which has not been reported earlier.

We also study the digital ionosonde data of Trivandrum (8.5°N, 77.0°E) station to understand the ionospheric condition at equatorial latitudes during the period of enhancement of OI 630 nm emission. In Fig. 12 ionospheric parameters, virtual height of the F2 layer, h'F (km) and square of the critical frequency of the F2 layer, f_0F2 are plotted at an interval of 15 min for three given nights as a function of IST h when BW was seen. The upper and lower panel in the figure shows the enhancement of electron density ($\sim f_0$F2)2 around midnight on March 13–14, and February 5–6, 2000. All three nights had equatorial spread-F (ESF) phenomena observed in f_0F2 as frequency spread F (Sp-F) and in h'F as range spread F (Sp-R). It is interesting to note that the MTM events reported here are all immediately preceded by ESF events commencing at 20:00 h when F-layer ($>$ 350 km) at Trivandrum was much higher than their average height in the evening hours. However, on the evening of February 5 at 20:15 h, the layer height rose up to 518 km and the rise of F-layer was very sharp and it gave rise to ESF phenomena. There was an abrupt enhancement of electron density on the night of March 13–14, 1999 and February 5–6, 2000 around the time of appearance of BW waves. Such a strong enhancement of electron density on the night of February 5 around middle of the night in the equatorial region leads us to believe that the event could be the manifestation of MTM. But the simultaneous measurement of F-region temperature at the equatorial region at night might have confirmed our results. However, on the night of April 19–20, f_0F2 values could not be measured around midnight due to the presence of ESF and h'F values showed undulations. Thus there could be some relationship between MTM and ESF events, which needs further detailed study at different longitude zones.

6. Conclusions

We have presented the results of the characteristics OI 630.0 nm all-sky-imaging observations carried out at a low-latitude station, Kolhapur, in India. Complementary ionosonde data were also used to study the formation and evolution of large-scale ionospheric plasma depletions and the study of brightness waves. The main results can be summarized as follows:

(a) The depletions were normally confined to the time between 21:30 and 01:00 h. There were simultaneous depletions observed in all three oxygen emission lines (OI 630.0, OI 557.7 and OI 777.4 nm) on the night of March 25, 1998. The depletions observed in OI 777.4 nm mean that the strong depletions have reached the height of the peak of the F2 layer. The width of the structures were varying between 50–350 km and often they were found to get tilted in the westward direction by about 30–40° during their movement towards east. Anderson and Mendillo (1983) attribute the westward tilt directly to the fact that, above F2 peak, the eastward plasma drift set up by the zonal wind decreases with altitude.

(b) By mapping the airglow depleted flux tubes along the geomagnetic field lines, plumes with heights 1500 km above equator have been observed. This height limit puts restriction on the capability of detecting bubbles attaining equatorial altitudes greater than 1500 km. The location of the observing station has to be moved more towards the north from the present position to detect very high rise (>1500 km) bubbles, which is a common feature at equatorial stations during high solar activity period.

(c) The mean F-region component to OI 557.7 nm emission was found to be 25 ± 4%. Takahashi et al. (1990) reported a value of 17% using simultaneous measurements of OI 630 and OI 557.7 nm emissions on board a rocket launched from an equatorial station at 5.8°S, 35.2°W in Brazil. It was further pointed out by Smith and Steiger (1968) that during the periods when OI 630 nm emission is enhanced, the F-region contribution to OI 557.7 nm also gets proportionately increased. The higher value (∼0.25) of the ratio r could be due to the enhanced OI 630 nm intensity, which is normally the case when strong plasma bubbles are developed in the low-latitude ionosphere. Also, the ratios are dependent on the height variations of the F-layer at the time of imaging observations.

(d) The average eastward plasma drift velocity was found to vary between 0 to 289 m/s. It matches well with drift estimate from scintillation, radar experiments and imaging observations (Fejer et al., 1981; Yeh et al., 1979; Sobral et al., 1985; Sinha and Raizada, 2000). We also found out that the ambient plasma (high-intensity bright region) and the plasma bubbles move eastward almost with the same speed. In the nighttime equatorial F-region, the eastward neutral wind develops a vertically downward polarization electric field which drives the plasma eastwards. In the absence of drainage of polarization charges, the neutral wind and E × B plasma drift become equal. Under these conditions the background plasma, the neutral and plasma bubbles will move eastwards with equal speed (Basu et al., 1996).

(e) The signature of midnight temperature maximum (MTM) was also obtained in 630.0 nm emission during the pre- and post-midnight hours of February 2000 and March and April 1999. Rao and Sastri (1994) reported the results on the characteristics of MTM for the Indian sector using the measurements of Doppler width of OI 630 nm night airglow at Kavalur (12.5°N, dip 9.5°N). Clear signature of MTM in enhancement of F-region neutral temperature was seen on 30% nights at the station during March–April 1992 and November 1992–April 1993.

The recent studies of MTM were made from Arequipa, Peru using an all-sky camera for OI 630 nm oxygen airglow (Mendillo et al., 1997). They found that pre-midnight brightness wave (PMBW) moves equatorward, while the post midnight brightness wave moves polewards. The average poleward speed for October 1993 midnight event was 248 m/s while the average speed for October, 1994 event was 368 m/s. However, our results show the movement of BW waves towards the north and northeast direction both during pre- and post-midnight hours with velocities ranging between 150 and 248 m/s, respectively, showing considerable agreement with earlier results. There was also change in the orientation of the BW structure from 30° to 45° towards west.

This work has also supported the view that the bubble generation is mostly associated with a strong development of equatorial ionization anomaly (EIA). An enhanced intensity in the region of reverse anomaly moving towards south from north was found to occur on most of the nights accompanied by bubble generation process.

Acknowledgements

The all-sky camera has been developed with the collaboration of Prof. M. Mendillo and his group at Boston University, Boston, UA. The authors are grateful to Prof. M. Mendillo for his continued interest in the project. Department of Science and Technology (DST), Government of India, New Delhi, funded the research in upper atmospheric science in IIG. The authors are grateful to Dr. C.V. Devasia (SPL, Trivandrum) for providing the ionosonde data of equatorial station, Trivandrum. The nightglow observations at Kolhapur were carried out under scientific collaboration program between IIG, Mumbai and Shivaji University, Kolhapur. Technical support received from Mr. P.T. Patil, Mr. S.H. Mahajan and Mr. L. Carlo in Airglow work is gratefully acknowledged.

References

Aarons, J., 1991. The role of the ring current in the generation or inhibition of equatorial F layer irregularities during magnetic storms. Radio Science 26 (4), 1131–1149.

Abdu, M.A., 1993. Equatorial spread-F and ionosphere–thermosphere system: a review. Trends in Geophysics Research 2, 193–209.

Abreu, V.J., Skinner, W.R., 1989. Inversion of Fabry–Perot CCD images: application to Doppler shift measurements. Applied Optics 28, 3382–3388.

Anderson, D.N., Mendillo, M., 1983. Ionospheric conditions affecting the evolution of equatorial plasma depletions. Geophysical Research Letters 10, 541–544.

Basu, Shantimoy., Basu, Sunanda., Kudeki, E., Zengingonul, H.P., Biondi, M.A., Meriwether, J.W., 1991. Zonal irregularity drifts and neutral winds measured near magnetic equator in Peru. Journal of Atmospheric and Terrestrial Physics 53, 743–755.

Basu, S, et al., 1996. Scintillations, plasma drifts and neutral winds in the equatorial ionosphere after sunset. Journal of Geophysical Research 101, 26,795–26,809.

Bates, D.R., 1981. The green light of the night sky. Planetary and Space Sciences 29, 1061–1067.

Baumgardner, J., Karandanis, S., 1984. CCD system using video graphics controller. Electronic Imaging 3, 28–31.

Biondi, M.A., Meriwether Jr., J.W., Fejer, B., Woodman, R., 1988. Measurements of the dynamics and coupling of the equatorial thermosphere and the F-region ionosphere over Peru. Journal of Atmospheric and Terrestrial Physics 50, 937–942.

Bittencourt, J.A., Teixeira, N.R., Sahai, Y., Takahashi, H., 1983. Mapping of ionospheric F-region parameters from atomic oxygen airglow emissions. Journal of Atmospheric and Terrestrial Physics 45, 697–705.

Chandra, H., Patel, V.P., Deshpande, M.R., Vyas, G.D., 1989. Spaced receiver scintillation measurements near magnetic equator. Indian Journal of Radio and Space Physics 18, 125–132.

Chiplunkar, M.W., Tillu, A.D., 1970. The F-layer component of the 5577 Å emission of the night airglow at Poona. Annales Geophysicae 26, 213–222.

Colerico, M., Mendillo, M., Notingham, D., Baumgardner, J., Meriwether, J., Mirik, J., Reinisch, B.W., Scali, J.L., Fesen, C.G., Biondi, M.A., 1996. Coordinated measurements of F region dynamics related to the thermospheric midnight temperature maximum. Journal of Geophysical Research 101, 26,783–26,793.

Dungey, J.W., 1956. Convective diffusion in the equatorial F region. Journal of Atmospheric and Terrestrial Physics 9, 304–310.

Fagundes, P.R., Sahai, Y., Takahashi, H., 1995. Investigations of OI 557.7 nm and 630 nm nightglow intensity ratios during the occurrence of equatorial F-region plasma bubbles. Journal of Atmospheric and Terrestrial Physics 57 (8), 929–932.

Fagundes, P.R., Sahai, Y., Batista, I.S., Abdu, M.A., Bittencourt, J.A., Takahashi, H., 1999. Observations of day-to-day variability in precursor signatures in equatorial F-region plasma depletions. Annales Geophysicae 17, 1053–1063.

Fejer, B.G., Farley, D.T., Gonzales, C.A., Woodman, R.F., Calderon, C., 1981. F-region east west drifts at Jicamarca. Journal of Geophysical Research 86, 215–218.

Fejer, B.J., de Paula, E.R., Ganzales, S.A., Woodman, R.F., 1991. Average vertical and zonal F-region plasma drifts over Jicamarca. Journal of Geophysical Research 96, 13,901–13,907.

Hedin, A.E., Biondi, M.A., Burnside, R.G., Hernandez, G., Johnson, R.M., Killeen, T.L., Mazaudier, C., Meriwether, J.W., Salah, J.E., Sica, R.J., Smith, R.W., Spencer, N.W., Wickwar, V.B., Virdi, T.S., 1991. Revised global model of thermosphere winds using satellite and ground based observations. Journal of Geophysical Research 96, 7657–7688.

Hedin, A.E., Fleming, E.L., Manson, A.H., Schmidin, F.J., Avery, S.K., Clark, R.R., Franke, S.J., Fraser, C.J., Tsuda, T., Vial, F., Vincent, R.A., 1996. Empirical wind model for the upper, middle and lower atmosphere. Journal of Geophysical Research 58 (13), 1421–1427.

Herrero, F.A., Spencer, N.W., 1982. On the horizontal distribution of the equatorial thermospheric midnight temperature maximum and its seasonal variation. Geophysical Research Letters 9, 1179–1183.

Herrero, F.A., Spencer, N.W., Mayr, H.G., 1993. Thermosphere and F-region plasma dynamics in the equatorial region. Advances in Space Research 13 (1), 200–220.

Janesick, J., Blouke, M., 1987. Sky on a chip: the fabulous CCD. Sky and Telescope 9, 238–242.

Kil, H., Heelis, R.A., 1998. Global distribution of density irregularities in the equatorial ionosphere. Journal of Geophysical Research 103, 407–417.

Koparkar, P.V., 1988. Drift of ionospheric irregularities at subtropical latitudes. Annales Geophysicae 6, 201–204.

Kumar, S., Gwal, A.K., Pathan, B.M., Rao, D.R.K., 1995. Zonal drift of ionospheric irregularities at temperate latitude in the Indian region. Annales Geophysicae 13, 724–7299.

Malcolm, R., Miles, C., Tinsley, B.A., 1984. Field aligned observations of trans-equatorial bubbles from Rarotonga in 1969–1970. Geophysical Research Letters 11 (7), 665–668.

Martyn, D.F., 1959. The normal F-region of the ionosphere. Proceedings of the IRE 47, 147–155.

Mendillo, M., Baumgardner, J., 1982. Airglow characteristics of equatorial plasma depletions. Journal of Geophysical Research 87, 7641–7652.

Mendillo, M., Tyler, A., 1983. Geometry of depleted plasma regions in the equatorial ionosphere. Journal of Geophysical Research 88, 5778–5782.

Mendillo, M., Baumgardner, J., Sultan, P.J., 1989. Optical and radar techniques applied to chemical release in active experiments in the ionosphere/thermosphere system. Advances in Space Research 10, 8–15.

Mendillo, M., Baumgardner, J., Colerico, M., Nottingham, D., 1997. Imaging science contributions to equatorial aeronomy: initial results from the MISETA program. Journal of Atmospheric and Terrestrial Physics 59, 1587–1599.

Mukherjee, G.K., 2002. Mapping of the simultaneous movement of the equatorial ionization anomaly (EIA) and ionospheric plasma bubbles through all-sky imaging of OI 630 nm emission. Terrestrial Atmospheric and Oceanic Sciences 13, 53–64.

Mukherjee, G.K., Dyson, P.L., 1992. A filter tilting photometer for nightglow measurement of 630.0 nm emission line. Indian Journal of Radio and Space Physics 21, 212–217.

Mukherjee, G.K., Carlo, L., Mahajan, S.H., Patil, P.T., 1998. First results of all-sky imaging from India. Earth Planets Space 50, 119–127.

Nakamura, T., Higashikawa, A., Tsuda, T., Matsushita, Y., 1999. Seasonal variations of gravity wave structures in OH airglow with a CCD imager at Shigaraki. Earth Planets Space 51, 897–906.

Peterson, V.L., Van Zandt, T.E., 1969. O (^{1}D) quenching in the ionospheric F-region. Planetary and Space Science 17, 1725–1736.

Rao, V.R., Kulkarni, P.V., 1974. Covariation of 6300 Å and 5577 Å emissions in tropical night airglow. Annales Geophysicae 30, 291–300.

Rao, H.R.N., Sastri, J.H., 1994. Characteristics of the equatorial midnight temperature maximum in the Indian sector. Annales Geophysicae 12, 276–278.

Rishbeth, H., 1971. The F-layer dynamo. Planetary and Space Science 19, 263–267.

Rohrbaugh, R.P., Hansen, W.B., Tinsley, B.A., Crain, B.L., McClure, J.P., Broad foot, A.L., 1989. Images of trans equatorial bubbles based on field-aligned airglow observations from Haleakela in 1984–1986. Journal of Geophysical Research 94, 6763–6770.

Sahai, Y., Aarons, J., Mendillo, M., Baumgardner, J., Bittencourt, J.A., Takahashi, H., 1994. OI 630 nm imaging observations of equatorial plasma depletions at 16°S latitude. Journal of Atmospheric and Terrestrial Physics 56, 1461–1475.

Sahai, Y., Bittencourt, J.A., Sobral, J.H.A., Fagundes, P.R., Takahashi, H., 1996. Observations of ionospheric plasma depletions using OI 630.0 nm nightglow imaging. Revista Brasil de Geophysics 14 (1), 15–28.

Singh, S., Johnson, F.S., Power, R.A., 1997. Gravity wave seeding of equatorial plasma bubbles. Journal of Geophysical Research 102, 7399–7410.

Sinha, H.S.S., Raizada, S., 2000. Some new features of ionospheric plasma depletions over the Indian zone using all-sky optical imaging. Earth Planets Space 52, 549–559.

Sinha, H.S.S., Rajesh, P.K., Misra, R.N., Dutt, N., 2001. Multi-wavelength imaging observations of plasma depletions over Kavalur, India. Annales Geophysicae 19, 1119–1131.

Smith, L.L., Steiger, W.R., 1968. Night airglow intensity variation in the [OI] 5577 A, [OI] 6300 Å and NaD 5890–96 Å emissions. Journal of Geophysical Research 73, 2531–2538.

Sobral, J.H.A., Abdu, M.A., Sahai, Y., 1985. Equatorial plasma bubble eastward velocity characteristics from scanning airglow photometer measurements over Cachoeira Paulista. Journal of Atmospheric and Terrestrial Physics 47, 895–900.

Sobral, J.H.A., Takahashi, H., Abdu, M.A., Muralikrishna, P., Sahai, Y., Zamlutti, C.J., 1992. O (^{1}S) and O (^{1}D) quantum yields from rocket measurements of electron densities and 557.7 and 630 nm emissions in the nocturnal F region. Planetary and Space Science 40, 607–619.

Spencer, N.W., Carignan, G.R., Mayr, H.G., Nieman, H.B., Theis, R.F., Wharton, L.E., 1979. The midnight temperature maximum in the Earth's equatorial thermosphere. Geophysical Research Letters 6, 444–446.

Takahashi, H., Clemesha, B.R., Bapista, P.P., Sahai, Y., Abdu, M.A., Muralikrishna, P., 1990. Equatorial F-region OI 6300 Å and OI 5577 Å emission profiles observed by rocket borne airglow photometers. Planetary and Space Science 38, 547–554.

Taylor, M.J., Eccles, J.V., LaBelle, J., Sobral, J.H.A., 1997. High resolution OI (630 nm) image measurements of F-region depletion drifts during Guara Campaign. Geophysical Research Letters 13, 1699–1702.

Tinsley, B.A., Bittencourt, J.A., 1975. Determination of F region height and peak electron density at night using airglow emissions from atomic oxygen. Journal of Geophysical Research 80, 2333–2337.

Tinsley, B.A., Rohrbaugh, R.P., Hanson, W.B., 1997. Images of transequatorial F region bubbles in 630 and 7774-nm emissions compared with satellite measurements. Journal of Geophysical Research 102, 2057–2077.

Tsunoda, R.T., 1985. Control of the seasonal and longitudinal occurrence of equatorial scintillation by the longitudinal gradient in integrated E-region Pederson conductivity. Journal of Geophysical Research 90, 447–456.

Weber, E.J., Bachau, J., Eather, R.H., Mende, S.B., 1978. North south aligned equatorial airglow depletions. Journal of Geophysical Research 83, 712–716.

Weber, E.J., Bachau, J., Moore, J.G., 1980. Airborne studies of equatorial F-layer ionospheric irregularities. Journal of Geophysical Research 85, 4631–4641.

Weber, E.J., Brinton, H.C., Bachau, J., Moore, J.G., 1982. Coordinated airborne and satellite measurements of equatorial plasma depletions. Journal of Geophysical Research 87, 10,503–10,513.

Weber, E.J., Aarons, J., Johnson, A.L., 1983. Conjugate studies of an isolated equatorial region. Journal of Geophysical Research 88, 3175–3180.

Yeh, K.C., Soicher, H., Liu, C.H., Bonelli, E., 1979. Ionospheric bubbles observed by the Faraday rotation method at Natal, Brazil. Geophysical Research Letters 6, 473–475.